KINEMATICS AND STATICS ANALYSIS OF A NOVLE 4-DOF PARALLEL MECHANISM FOR LASER WEEDING ROBOT

/

基于激光除草机器人的一种新型 4 自由度并联机构运动学和静力学分析

Ph.D. Wang Xuelei, Ph.D. Huang Jie, Ph.D. Zhao Dongjie, Ph.D. Guo Honghong, Ph.D. Li Chuanjun, Prof. Zhang Bin*)
College of Engineering, China Agricultural University, Beijing / China
Tel: +8615650715561; E-mail: zhangbin64@cau.edu.cn

Keywords: *parallel mechanism, kinematics, statics, inverse/forward velocities*

ABSTRACT

To eliminate the serious threat of weeds to farmland crops, this study proposes a laser weeding robot based on a novel 3UPS-RPU parallel mechanism (PM). The robot uses laser thermal effects to eliminate weeds in crop rows. The novel 3UPS-RPU PM is composed of three UPS-type active legs and one RPU-type active leg. Approaches for solving the inverse kinematics, inverse/forward velocities, inverse/forward accelerations, active forces, and constrained forces of this PM are derived and unified for other PMs with linear active legs. The kinematic curves demonstrate that the input of active legs 1 and 3 are consistent, while the moving platform moves according to a line-type translational movement which is the unique characteristic of the proposed PM. The active legs move according to a non-linear motion law, while the moving platform of the PM moves according to a line-type patterns, which is a common characteristic. The kinematic curves show that this PM has steady movement with no sudden changes or breakpoints which satisfies the stability requirements for the laser in the robot. Theoretical formulas and results provide a basis for the optimization of the structure design, control, dynamic performance analysis, manufacturing, and applications of the 3UPS-RPU PM.

摘要

为消除杂草对农作物的严重影响，论文提出了基于一种新型 4 自由度并联机构的激光除草机器人，该机器人利用激光的热效应来消除农作物中的杂草。新型并联机构包括 3 个 UPS 主动件和 1 个 RPU 主动件。论文推导了该并联机构的运动学反解，速度，加速度，主动力和约束力公式，本推导方法同样适用于其他由直线主动件控制的并联机构。当 3UPS-RPU 并联机构动平台只有平移运动时，主动件 1 和 3 的运动实时同步，这是本机构特有的性质。当动平台按照线性方式运动时，四个主动件为非线性运动，这也是并联机构共有的特性。从运动学曲线可以看出该机构运动平稳，运动过程中没有突变和断点，满足该激光除草机器人对激光束稳定性的要求。理论方程和结果为机构的优化设计、控制、动力学性能分析、制作和应用提供了基础。

INTRODUCTION

Farmland weeds grow and spread easily thus compete for different resources, such as moisture, nutrients, sunlight and space, that crops need to grow. Weeds also become sources of infection through pathogenic bacteria, which seriously affect the normal growth of crops, resulting in the decrease in yield and quality.

Chemical weed control has always been used in traditional agricultural production and has been proven to have harmful side-effects *(Martins et al., 2016; Nath et al., 2016; Datsch Silveira et al., 2016)*. *(Datsch Silveira et al., 2016)* evaluated the mutagenic effects of two herbicides, namely, Clorimurom Nortox® and Imazaquim Ultra Nortox®, which are widely used on soybean crops in Brazil. Allium cepa assay was used as the test system. The two herbicides caused mutagenic damages in the Allium cepa cells, which implied the need for careful handling of these products to minimize the risk of human and environmental contamination. Ecotoxic effects of commonly used herbicides i.e. glyphosate, atrazine, metribuzin and alachlor were evaluated on the biological and demographic parameters of Zygogramma bicolorata Pallister on parthenium in laboratory by Hasan *(Hasan et al., 2016)* Based on the present study, none of the tested herbicide can be classified as safe to Zygogramma bicolorata, while glyphosate was found to be least toxic. Therefore, this weeding process not only affects the growth of crops but also pollutes the soil, resulting in herbicide wastes—a serious threat to the health of farmland workers. Furthermore, the safety of agricultural products is also affect by the drug residue.

Mechanical weed control was developed to replace its chemical counterpart, which utilizes standard tools, such as field hoes to weed. *(Cordill et al., 2011)* proposed a mechanical weed control machine containing a sensing arrangement, control algorithm and dual mechanical end effectors was successfully developed and tested. The overall functionality of the machine was proven, but the percentage of fatally damaged plants was 8.8% in the absence of weeds and reaching 23.7% in heavy weed infested areas with hundreds of weeds per m^2. *(Pérez-Ruiz et al., 2012)* described a fully automatic intra-row mechanical weed knife path control system for transplanted row crops. A real-time kinematics global positioning system (GPS) was used to automatically detect crop planting positions and to control the path of a pair of intra-row weed knives travelling between crop plants along row centerline. *(Pérez-Ruiz et al., 2014)* also described the development and in-field assessment of an automatic intra-row, hoe-based weeding co-robot system with real-time pneumatic hoe actuation based on an accurate odometry sensing technique. In this work, mechanical weed control was achieved by a co-robot actuator that automatically positioned a pair of miniature hoes into the intra-row zone between crop plants.

However, mechanical damage to crop seedlings can be easily inflicted because of the restriction of the movement precision of mechanical weeding devices. The soils turned over by mechanical weeding device tend to bury the seedlings. Moreover, weed seeds may be spared from mechanical weeding, which may lead to their re-germination.

Currently, concerning about the impact of eco-agriculture from western countries, a growing number of consumers demand natural food with little to no chemicals because of the eco-agricultural effect from Western countries. Automated, non-chemical, intra-row weed control techniques for crop production systems have become a necessary challenge for industrialized countries. To satisfy the needs of the market, new methodologies need to be developed to produce satisfactory outcomes without damaging the environment. Therefore, this research presents a laser weeding robot that does not rely on chemical resources.

In recent years, PMs have been extensively studied and applied because of their high durability, lower manufacturing cost, simple structure, large bearing capacity and easy to control, etc *(Ganesh et al., 2015; Li et al., 2016; Yang et al., 2016)*. Various PMs have been used in fields such as walking legs, parallel machine tools, rehabilitation robots, industrial robots, heavy-duty forging manipulators, etc *(Jiang et al., 2016; Lin et al., 2016; Song et al., 2016)* . Generally, PMs with four degree of freedom (4-DoF) have attracted significant attentions because they are simpler in structure, easier manufacture, cheaper, and more sustainable than PMs with 6-DoF *(Dong et al., 2016; He et al., 2015)* . To create some novel 4-DoF PMs and investigate their kinematic characteristics have great significances in current industrial manufacturing and other fields.

However, up to now, no study have been found existed on 3UPS-RPU PM with two rotations and two translations and this is the first time that PMs will be used in laser weeding robot. This research focuses on the kinematics and statics analysis of the proposed PM and proposes a unified method for solving the kinematics and statics of PMs with linear active legs because a 3-UPS-RPU PM is the basis for the laser weeding robot. In addition, this paper provides a theoretical basis for its optimum structural design, control, manufacturing, and different applications.

MATERIAL AND METHODS

Description of the Laser Weeding Robot

The laser weeding robot uses laser thermal effects to eliminate weeds in crop rows. The main robot components are the frame, a 3UPS-RPU 4-DoF PM, a laser, a control system, batteries, and two vision systems, as illustrated in Figure 1.

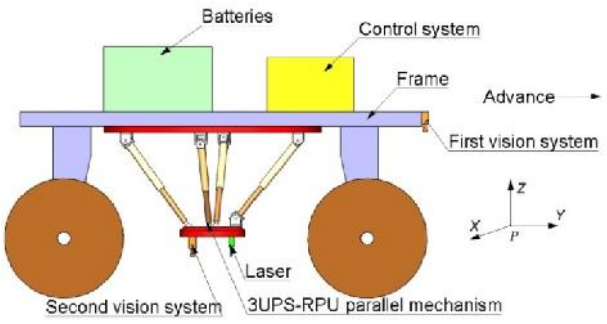

Fig. 1 - Scheme of the laser weeding robot

The 3UPS-RPU PM is held over the frame and trailed by a conventional tractor. The first vision system is placed in the front of the tractor to detect weeds in real time and send their coordinates to the control system while the robot is in motion. A secondary vision camera is used to improve robot precision and it is placed close to the laser. Its mission is to correct inertial perturbations by relocating every individual weeds detected by the first vision system.

The 3UPS-RPU PM is composed of a moving platform, a fixed base, three UPS-type (U represents universal joint, P represents prismatic joint, S represents spherical joint) active legs and one RPU-type (R represents revolute joint) active leg with the linear actuators, see Figure 2. Since each of the active legs with the linear actuator only bears the axial force that along its own axis, it has a larger capacity of load bearing and is simple in structure.

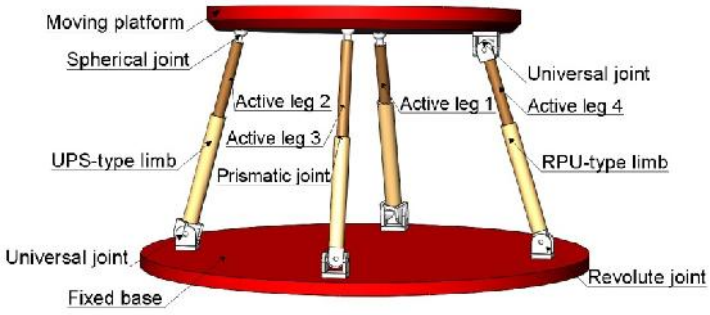

Fig. 2 - The 3UPS-RPU parallel mechanism

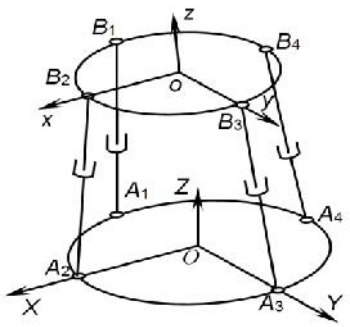

Fig. 3 - Schematic model of 3UPS-RPU PM

In the 3UPS-RPU PM, the number of independent common constraints is λ= 0; the order of mechanism is d = 6 - λ = 6; the number of links is n =10 including one moving platform, four cylinders, four piston-rods and one fixed base; the number of joints is g = 12, including three universal joints, four prismatic joints, four spherical joints and one revolute joint; the DoFs of the joints are f_P = f_R = 1 for prismatic or revolute joint, f_U= 2 for universal joint, f_S = 3 for spherical joint; the number of redundant constraints is v = 0; the redundancy DoFs is ζ = 0. Based on the revised Kutzbach-Grübler equation *(Huang et al., 1997)*, the DoF of the 3UPS-RPU PM is calculated as

$$M = d\left(n - g - 1\right) + \sum_{i=1}^{g} f_i + v - \zeta = 6 \times \left(10 - 12 - 1\right) + \left(2 \times 3 + 4 \times 1 + 3 \times 3 + 2 \times 1 + 1 \times 1\right) = 4 \qquad (1)$$

Thus, the 3UPS-RPU PM has four DoFs with two translational DoFs and two rotational DoFs.

In the laser weeding robot illustrated in Figure1, the Y axis of the coordinate system P-XYZ is along the advance direction of the robot, Z axis is perpendicular to the frame, while X axis is confirmed by the right-hand rule. The 3UPS-RPU 4-DoF PM can achieve movements along the Y and Z axes directions and rotations around the X and Y axes. Among them, the movement along the Y axis is used to compensate for the positional change of the weeds so that the laser beams of the robot will remain stationary to the weeds. The movement along the Z axis allows the robot to work in the field with different crop heights, greatly improving the working space. With its simple structure, the laser weeding robot can be used in different height or line spacing crops without the risk of burying seedlings and damaging crops.

Analysis of 3UPS-RPU PM

The coordinate system O-XYZ is fixed at the centre of the fixed base at O, and o-xyz is fixed at the centre of the moving platform at o, as illustrated in Figure 3. A_i (i=1, 2...4) are equally distributed around a circle with a radius of r_a on the fixed base. B_i (i=1, 2…4) are uniformly distributed around a circle with a radius of r_b on the moving platform. At the initial time, the coordinate systems O-XYZ and o-xyz are parallel, and Z-axis is coincident with z-axis.

Before analyzing the inverse kinematics of the 3UPS-RPU PM, the position of A_i (i =1, 2…4) in O-XYZ, B_i (i =1, 2…4) in o-xyz, and B_i (i=1, 2…4) in O-XYZ must be determined, and they can be expressed as:

$$A_i = \begin{bmatrix} A_{iX} \\ A_{iY} \\ A_{iZ} \end{bmatrix}, \quad B_i = \begin{bmatrix} B_{ix} \\ B_{iy} \\ B_{iz} \end{bmatrix}, \quad B_i^O = \begin{bmatrix} B_{iX} \\ B_{iY} \\ B_{iZ} \end{bmatrix}, \quad R_o^O = \begin{bmatrix} l_x & m_x & n_x \\ l_y & m_y & n_y \\ l_z & m_z & n_z \end{bmatrix},$$

$$o=\begin{bmatrix} X_o \\ Y_o \\ Z_o \end{bmatrix}, \quad B_i^O = R_o^O B_i + o \quad (i=1, 2\ldots4) \tag{2}$$

Where $o=[\,X_o\ Y_o\ Z_o\,]^T$ is the position vector of *o-xyz* in *O-XYZ*, matrix R_o^O is a rotation transformation matrix from *o-xyz* to *O-XYZ* and it's formed by two Euler rotations of (*x* y_1), namely, a rotation of *α* about *x*-axis, followed by a rotation of *β* about y_1-axis, where y_1 is formed by *y* rotating about *x* by *α*. Let *λ* be one of (*α*, *β*) and set *cλ*= cos*λ*, s*λ*= sin*λ*, thus, R_o^O is derived as follows:

$$R_o^O=\begin{bmatrix} c\beta & 0 & s\beta \\ s\alpha s\beta & c\alpha & -s\alpha c\beta \\ -c\alpha s\beta & s\alpha & c\alpha c\beta \end{bmatrix}$$

Each active leg, $\boldsymbol{l_i}$ (*i* = 1, 2…4) can be expressed as:

$$l_i = B_i^O - A_i \tag{3}$$

Thus, the formula for solving $\boldsymbol{l_i}$ (*i* = 1, 2…4) are derived as:

$$l_i^2=\left|B_i^O-A_i\right|^2 \Rightarrow \begin{cases} l_1^2=\left|B_1^O-A_1\right|^2 \\ \quad =X_o^2+\left(-r_b c\alpha+r_a+Y_o\right)^2+\left(-r_b s\alpha+Z_o\right)^2 \\ l_2^2=\left|B_2^O-A_2\right|^2 \\ \quad =\left(r_b c\beta+X_o-r_a\right)^2+\left(r_b s\alpha s\beta+Y_o\right)^2+\left(-r_b c\alpha s\beta+Z_o\right)^2 \\ l_3^2=\left|B_3^O-A_3\right|^2 \\ \quad =X_o^2+\left(r_b c\alpha+Y_o-r_a\right)^2+\left(r_b s\alpha+Z_o\right)^2 \\ l_4^2=\left|B_4^O-A_4\right|^2 \\ \quad =\left(-r_b c\beta+X_o+r_a\right)^2+\left(-r_b s\alpha s\beta+Y_o\right)^2+\left(r_b c\alpha s\beta+Z_o\right)^2 \end{cases} \tag{4}$$

The unit vector n_i of l_i (*i* = 1, 2…4) can be derived as:

$$n_i=\frac{l_i}{l_l}=\frac{1}{l_i}\begin{bmatrix} B_{iX}-A_{iX} \\ B_{iY}-A_{iY} \\ B_{iZ}-A_{iZ} \end{bmatrix} \tag{5}$$

Let *V* and v_i be the velocities of the moving platform at *o* and B_i, respectively, written as:

$$V=\begin{bmatrix} v \\ \mu \end{bmatrix}_{6\times1},\ v=\begin{bmatrix} v_x \\ v_y \\ v_z \end{bmatrix},\ \omega=\begin{bmatrix} \omega_x \\ \omega_y \\ \omega_z \end{bmatrix},\ v_i=v+\omega\times r_i \quad (i=1, 2\ldots4) \tag{6}$$

Where *v* and *ω* are the velocity and angular velocity of *o-xyz* at *o*, r_i (*i*=1, 2…4) are the vectors from point *o* to B_i. Through Equation (6), the velocities along the active legs l_i (*i* = 1, 2…4) are derived as follows:

$$v_{li}=v_i\cdot n_i=\left(v+\omega\times r_i\right)\cdot n_i=n_i\cdot v+\left(r_i\times n_i\right)\cdot\omega \qquad (i=1, 2\ldots4) \tag{7}$$

$$\Rightarrow\begin{bmatrix} v_{l_1} \\ v_{l_2} \\ v_{l_3} \\ v_{l_4} \end{bmatrix}=\begin{bmatrix} n_1^T & \left(r_1\times n_1\right)^T \\ n_2^T & \left(r_2\times n_2\right)^T \\ n_3^T & \left(r_3\times n_3\right)^T \\ n_4^T & \left(r_4\times n_4\right)^T \end{bmatrix}_{4\times6}\cdot\begin{bmatrix} v \\ \omega \end{bmatrix}_{6\times1} \tag{8}$$

The force situation of the 3UPS+RPU PM is shown in Figure 4. Constrained force F_U, which is applied on the moving platform, is in parallel to the revolute joint R of the RPU limb.

The restriction moment M_U, applied on the moving platform, is parallel to the *z*-axis. Let n_5 be the unit vector of revolute joint *R*, and n_6 be the unit vector of *z*-axis.

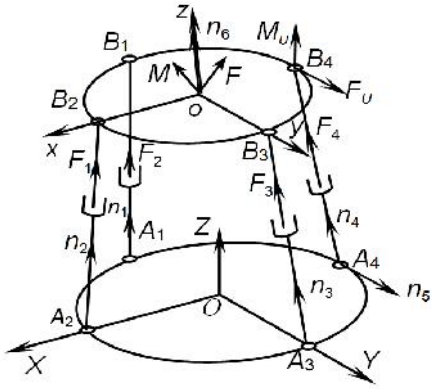

Fig. 4 - The force situation of the 3UPS + RPU PM

Since constrained force F_U and restriction moment M_U don't do any work during the movement of moving platform, there must be:

$$F_U n_5 \cdot v + (r_4 \times F_U n_5) \cdot \omega = 0, \quad (M_U n_6) \cdot \omega = 0 \quad \Rightarrow \begin{bmatrix} n_5^T & (r_4 \times n_5)^T \\ 0_{1\times 3} & n_6^T \end{bmatrix}_{2\times 6} \cdot V = \begin{bmatrix} 0 \\ 0 \end{bmatrix} \tag{9}$$

By combining Equations (8) and (9), the formula for solving the inverse/forward velocities and the Jacobian matrix *G* are derived as follows:

$$\Rightarrow \begin{bmatrix} v_{l_1} \\ v_{l_2} \\ v_{l_3} \\ v_{l_4} \\ 0 \\ 0 \end{bmatrix} = G \cdot V, \quad V = G^{-1} \cdot \begin{bmatrix} v_{l_1} \\ v_{l_2} \\ v_{l_3} \\ v_{l_4} \\ 0 \\ 0 \end{bmatrix}$$

$$\Rightarrow G = \begin{bmatrix} n_1^T & (r_1 \times n_1)^T \\ n_2^T & (r_2 \times n_2)^T \\ n_3^T & (r_3 \times n_3)^T \\ n_4^T & (r_4 \times n_4)^T \\ n_5^T & (r_4 \times n_5)^T \\ 0_{1\times 3} & n_6^T \end{bmatrix}_{6\times 6} \tag{10}$$

Let *A* be the acceleration of the moving platform at *o*. Let *a* and *ε* be a linear acceleration and an angular acceleration of moving platform at *o*, respectively.

They can be expressed as follows:

$$A = \begin{bmatrix} a \\ £ \end{bmatrix}_{6\times 1} \qquad a = \begin{bmatrix} a_x \\ a_y \\ a_z \end{bmatrix}, \quad \varepsilon = \begin{bmatrix} \varepsilon_x \\ \varepsilon_y \\ \varepsilon_z \end{bmatrix} \tag{11}$$

Suppose there are two vectors η, , and a skew-symmetric matrix ¦ .There must be the following relevant Equations *(Huang et al., 1997)*:

$$\eta = \begin{bmatrix} \eta_x \\ \eta_y \\ \eta_z \end{bmatrix}, \quad \zeta = \begin{bmatrix} \zeta_x \\ \zeta_y \\ \zeta_z \end{bmatrix}, \quad \hat{\eta} = \begin{bmatrix} 0 & -\eta_z & \eta_y \\ \eta_z & 0 & -\eta_x \\ -\eta_y & \eta_x & 0 \end{bmatrix}, \quad \eta \times \zeta = \hat{\eta}\zeta, \quad \hat{\eta}^T = -\hat{\eta} \tag{12}$$

By differentiating the first four rows of Equation (10) with respect to time, four accelerations $\boldsymbol{a}_{l_i}$ along the i^{th} active leg are expressed as follows:

$$a_{l_i} = \left[n_i^T \quad (r_i \times n_i)^T \right] A + V^T H_i V \quad (i=1, 2\ldots4) \tag{13}$$

Where $$H_i = \frac{1}{l_i}\begin{bmatrix} E_{3\times3} & -\hat{r}_i \\ \hat{r}_i & -\hat{r}_i^2 \end{bmatrix}_{6\times6} - \frac{1}{l_i}\begin{bmatrix} n_i \\ r_i \times n_i \end{bmatrix}\left[n_i^T \quad (r_i \times n_i)^T \right] + \begin{bmatrix} 0_{3\times3} & 0_{3\times3} \\ 0_{3\times3} & \hat{r}_i \hat{n}_i \end{bmatrix}_{6\times6}.$$

By differentiating the fifth row of Equation (10) with respect to time, we obtain:

$$0_{1\times6} = \left[n_5^T \quad (r_4 \times n_5)^T \right] A + V^T H_5 V \tag{14}$$

Where $H_5 = \begin{bmatrix} 0_{3\times3} & 0_{3\times3} \\ 0_{3\times3} & -\hat{r}_4 \hat{n}_5 \end{bmatrix}_{6\times6}$.

By differentiating the sixth row of Equation (10) with respect to time, we obtain:

$$0_{1\times6} = \left[0_{1\times3} \quad n_6^T \right] A + V^T H_6 V \tag{15}$$

Where, $H_6 = \begin{bmatrix} 0_{3\times3} & 0_{3\times3} \\ 0_{3\times3} & J_\alpha \end{bmatrix}_{6\times6}$, $J_\alpha = \begin{bmatrix} c\beta & 0 & 0 \\ s\alpha s\beta & c\alpha & 0 \\ -c\alpha s\beta & s\alpha & 1 \end{bmatrix}^{-1 T} \cdot \begin{bmatrix} 0 & -c\alpha c\beta & -s\alpha c\beta \\ c\beta & s\alpha s\beta & -c\alpha s\beta \\ 0 & 0 & 0 \end{bmatrix}$

Combining Equations (13) with (14) and (15), an inverse acceleration a_{in}, a forward acceleration A, and a Hessian matrix H are derived as follows:

$$a_{in} = GA + V^T HV, \quad A = G^{-1}\left(a_{in} - V^T HV\right) \tag{16}$$

Where $a_{in} = \left[a_{l_1} \; a_{l_2} \; a_{l_3} \; a_{l_4} \; 0 \; 0 \right]^T$ and $H = \left[H_1 \; H_2 \; H_3 \; H_4 \; H_5 \; H_6 \right]^T$.

Active/Constraint Forces and Torque

The 3UPS-RPU PM is an ideal constrained system when the gravity and friction of all the links are ignored, and its workload can be simplified as a wrench (F, M) applied on the moving platform at o, where F is the central force and M is the central torque. (F_X, F_Y, F_Z, M_X, M_Y, M_Z) are the components of (F, M) and they are balanced by four active forces F_i (i=1, 2…4), one constrained force F_U, and one restriction moment M_U, each of F_i is applied on and along the active legs l_i (i=1,2…4).

Based on the principle of virtual work, and Equation (10), the formula for solving the active/constrained force and torque are derived as follows:

$$\begin{bmatrix} F_1 \\ F_2 \\ F_3 \\ F_4 \\ F_U \\ M_U \end{bmatrix}^T \cdot \begin{bmatrix} v_{r_1} \\ v_{r_2} \\ v_{r_3} \\ v_{r_4} \\ 0 \\ 0 \end{bmatrix} + \begin{bmatrix} F \\ T \end{bmatrix}^T \cdot V = 0, \quad \begin{bmatrix} F_1 \\ F_2 \\ F_3 \\ F_4 \\ F_U \\ M_U \end{bmatrix}^T \cdot G + \begin{bmatrix} F \\ T \end{bmatrix}^T = 0$$

$$\Rightarrow \begin{bmatrix} F_1 \\ F_2 \\ F_3 \\ F_4 \\ F_U \\ M_U \end{bmatrix} = -\left(G^{-1}\right)^T \begin{bmatrix} F \\ T \end{bmatrix} = -\left(G^T\right)^{-1} \begin{bmatrix} F \\ T \end{bmatrix} \tag{17}$$

Where, $-\left(G^T\right)^{-1}$ is defined as a force Jacobian matrix.

RESULTS

Results Analysis and Discussion

In the 3UPS-RPU PM, when given pose parameters of moving platform with respect to time, the length, velocity, acceleration of four active legs can be calculated. Set r_a = 400 mm, r_b = 300 mm, and the original distance between two platforms is H = 600 mm. Two cases are employed in analysis of the PM.

In case one, the moving platform is presumed to move according to a line-type translational movement, that is,

$$\begin{cases} \alpha = 0 \\ \beta = 0 \\ X_0 = 5 * t \\ Z_0 = 5 * t \end{cases} \tag{18}$$

Based on the relevant analytics of Equations (4), (10) and (16), the lengths, velocities and accelerations of the four active legs that over time are obtained through the Matlab software, and are presented in Figures 5(a), 5(b), and 5(c), respectively.

According to the results and data shown in Figure 5(a), the lengths of the four active legs are initially the same. As time goes by, the lengths of active leg 4 becomes the longest while active leg 2 becomes the shortest. According to the results and data shown in Figure 5(b), the velocity of active leg 4 is at a maximum while active leg 2 is constant at a minimum. According to the results and data shown in Figure 5(c), the acceleration of active leg 2 is at the maximum while active leg 4 is constantly at the minimum, but the values are greater than zero. The lengths, velocities, and accelerations of active legs 1 and 3 are always consistent with each other, and their values are between that of active legs 2 and 4, that is, the input of active legs 1 and 3 are always consistent. The results and data shown in Figure 5(a), 5(b), and 5(c) are consistent with the actual movement and in accordance with the geometric characteristics of PMs. The velocity and acceleration of the four active legs are changing all the time. Therefore, the movements of the PM are non-linear.

Case two is the presumption that the moving platform of the mechanism moves according to a line-type rotational movement, that is,

$$\begin{cases} \alpha = (\pi/90) * t \\ \beta = (\pi/90) * t \\ X_0 = 0 \\ Z_0 = 0 \end{cases} \tag{19}$$

Based on the relevant analytics of Equations (4), (10) and (16), the lengths, velocities and accelerations of the four active legs over time are obtained through the Matlab software, which are presented in Figures 5(d), 5(e), 5(f).

According to the results and data shown in Figure 5(d), the lengths of the four active legs are initially the same. As time goes by, the lengths of active legs 1 and 2 become shorter while those of active legs 3 and 4 become longer. According to the results and data shown in Figure 5(e), the velocities of active legs 1 and 2 gradually increase while those of active legs 3 and 4 continually decrease. According to the results and data shown in Figure 5(f), the accelerations of active legs 1 and 2 are always greater than zero, while those of active legs 3 and 4 are always less than zero. Moreover, the slopes of active legs 2 and 4 are larger than those of active legs 1 and 3. The results and data shown in Figures 5(d), 5(e), and 5(f) are consistent with the actual movement and in accordance with geometric characteristics of PMs. The velocities and accelerations of the four active legs shift at all times. Therefore, their movements are also non-linear two.

As a result, the moving platform of the PM moves according to line-type patterns, but all active legs move according to the non-linear motion law and all the PMs have the same Characteristics.

The kinematic diagrams show that the PM movement is steady and its displacement, velocity, and acceleration curves exhibit no sudden changes or breakpoints, illustrating the correctness of this PM, and satisfying the stability requirements for the laser in the robot.

Theoretical formulas and results provide a basis for the optimization of the structure design, control, dynamic performance analysis, manufacturing, and applications of the 3UPS-RPU PM.

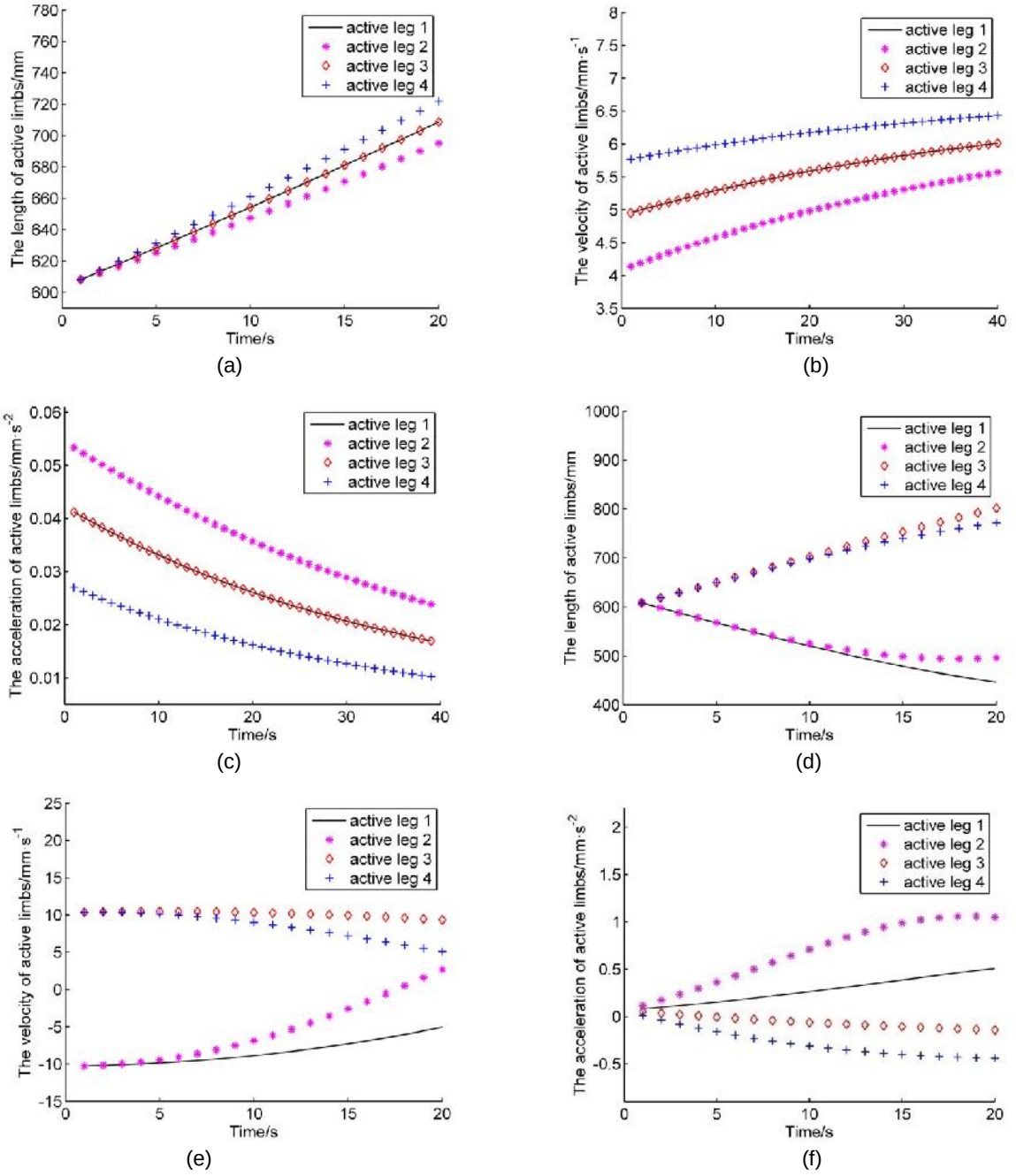

Fig. 5 - Kinematic analysis of active legs

CONCLUSIONS

With the increase in the demand for green vegetables and make up the inadequacies of Chemical and mechanical weeding, a more efficient method of weeding has become a necessity. This research demonstrated a laser weeding robot based on a novel 3UPS-RPU PM, which utilizes laser thermal effects to eliminate weeds in crop rows. This research focus on kinematics and statics analysis of the 3UPS-RPU PM as it is basis of the weeding robot. The conclusions are shown as follows:

(1) The approaches for solving the inverse/forward velocities and accelerations of the 3UPS-RPU PM were derived and unified for other PMs with linear active legs. The velocity Jacobian matrix and Hessian matrix derived can be used to analyze the kinematic singularity of PMs.

(2) The curves of the lengths, velocities, and accelerations of the four active legs showed that the movement of active legs 1 and 3 were consistent with each other, while the moving platform moved according to a line-type translational movement, which is a unique characteristic of the proposed PM. All active legs moved according to the non-linear motion law, while the moving platform of the PM moved according to a line-type pattern, which is a common characteristic of PMs. These results are used for the control system of the robot. The stability of the kinematic curves show that the PM satisfies the stability requirements for the laser in the robot. Thus, the weeding quality can be improved greatly.

(3) A simple approach for solving the active constrained forces of the 3UPS-RPU PM was derived based on the principle of virtual work, and this approach can be used on other PMs.

In addition, this paper provides a theoretical basis for the optimum structural design, control, manufacturing, and different applications of the robot. Future work should combine theoretical analysis with field experiments.

ACKNOWLEDGEMENT

This work is supported by the Doctoral Fund from the National Education Ministry of China no. 20120008110046. The authors would like to thank the reviewers for their critical reviews and suggestions to improve the clarity of this article. They would also like to thank the managing editor for the works on the manuscript.

REFERENCES

[1] Cordill C., Grift T. E., (2011), Design and testing of an intra-row mechanical weeding machine for corn, *Biosystems Engineering*, Vol.110, Issue 3, pp.247-252, *Academic Press Inc Elsevier Science*, San Diego/USA;

[2] Datsch Silveira M.A., Ribeiro D. L., Dos Datsch Santos T. A., et al., (2016), Mutagenicity of two herbicides widely used on soybean crops by the Allium cepa test, *Cytotechnolygy*, Vol.68, Issue 4, pp.1215-1222, Springer Netherlands, Dordrecht/Netherlands;

[3] Dong G., Sun T., Song Y. M., (2016), Mobility analysis and kinematic synthesis of a novel 4-dof parallel manipulator, *Robotica*, Vol.34, Issue 5, pp.1010-1025, Cambridge University Press, New York/USA;

[4] Ganesh S. S., Rao A. B. K., (2015), Inverse dynamics of a 3-DOF translational parallel kinematic machine, *Journal of Mechanical Science and Technology,* Vol.29, Issue 11, pp.4583-4591, Korean Society of Mechanical Engineers, Seoul/Korean;

[5] Hasan F., Shafiq Ansari M., (2016), Ecotoxicological hazards of herbicides on biological attributes of Zygogramma bicolorata Pallister (Coleoptera: Chrysomelidae), *Chemosphere*, Vol.154, pp.398-407, Pergamon, Elsevier Science Ltd, Oxford/England;

[6] Huang Z., Kong L. F., Fang Y. F., (1997), *Theory on Parallel Robotics and Control*, Machinery Industry Press, Beijing/China;

[7] He J., Gao F., Meng X. D., et al., (2015), Type synthesis for 4-dof parallel press mechanism using gf set theory*, Chinese Journal of Mechanical Engineering*, Vol.28, Issue 4, pp.851-859, Editorial Office of Chinese Journal of Mechanical Engineering, Beijing/China;

[8] Jiang X. L., Gosselin C., (2016), Trajectory generation for three-degree-of-freedom cable-suspended parallel robots based on analytical integration of the dynamic equations, *Journal of Mechanisms and Robotics-Transactions of the ASME*, Vol. 8, Issue 4, pp.1110-1117, American Society of Mechanical Engineers, New York/USA;

[9] Lin H. T., Chiang M. H., (2016), The integration of the image sensor with a 3-dof pneumatic parallel manipulator, *Sensors*, Vol.16, Issue 7, pp.1–17, Molecular Diversity Preservation International, Basel/Switzerland;

[10] Li B., Li Y. M., Zhao X. H., (2016), Kinematics analysis of a novel over-constrained three degree-of-freedom spatial parallel manipulator, *Mechanism and Machine Theory*, Vol.104, pp.222-233, Pergamon-Elsevier Science Ltd, Oxford/England;

[11] Martins D., Goncalves C. G., da S. J., et al., (2016), Winter mulches and chemical control on weeds in maize, *Revista Ciencia Agronomica*, Vol.47, Issue 4, pp.649-657, Universidade Federal do Ceará, Fortaleza/Brazil;

[12] Nath C. P., Das T. K., Rana K. S., (2016), Effects of herbicides and tillage practices on weeds and summer mungbean (Vigna radiata) in wheat (Triticum aestivum)-mungbean cropping sequence, *Indian Journal of Agricultural Sciences*, Vol.86, Issue 7, pp.860-864, Indian Council of Agricultural Research, New Delhi/ Indian;

[13] Pérez-Ruiz M., Slaughter D. C., Gliever C. J., et al., (2012), Automatic GPS-based intra-row weed knife control system for transplanted row crops, *Computers and Electronics in Agriculture*, Vol. 80, pp.41-49, Elsevier Science Ltd, Oxford/England;

[14] Pérez-Ruiz M., Slaughter D. C., Fathallah F. A., et al., (2014), Co-robotic intra-row weed control system, *Biosystems Engineering*, Vol.126, pp.45-55, Academic Press Inc Elsevier Science, San Diego/USA;
[15] Song Y. M., Zhang J. T., Lian B. B., et al., (2016), Kinematic calibration of a 5-dof parallel kinematic machine, *Precision Engineering*, Vol.45, pp.242–261, Elsevier Science Inc, New York/USA;
[16] Yang S. F., Sun T., Huang T., (2016), A finite screw approach to type synthesis of three-DOF translational parallel mechanisms, *Mechanism and Machine Theory*, Vol.104, pp.405-419, Pergamon-Elsevier Science Ltd, Oxford/England.